Third International Conference on CFD in the Minerals and Process Industries
CSIRO, Melbourne, Australia
10-12 December 2003

NUMERICAL STUDY OF THE EFFECT OF BLADE SZE ON PUMPING EFFECTIVENESS OF A PADDLE IMPELLER IN AN UNBAFFLED MIXING VESSEL

L. MUNUNGA, K. HOURIGAN and M. THOMPSON

Department of Mechanical Engineering, Monash University, Clayton Campus,
PO Box 31, Vic 3800, Australia

ABSTRACT

Numerical simulations of the flow field generated by a six-bladed paddle impeller in a closed unbaffled mixing vessel are presented. Computations were performed using the CFD software package FLUENT using grids generated from the pre-processor software package Gambit. The Rotating Frame Model was used in the solution process. Investigations were carried out over a range of Reynolds numbers covering laminar, transitional and turbulent flow regimes, while varying the axial dimension of the blade. Predicted flow field results have compared reasonably well with data from previous studies. It was found that increases in blade width (Wb) have resulted in corresponding increases in flow number (Nq), power number (Np) and pumping efficiency (λ_p), at least for the range of blade widths covered here. For all Wb's considered here, Np was highest in the laminar region and lowest in the turbulent region, whereas Nq was highest in the transitional regime. Pumping effectiveness (η_e) was found to maintain constant values of 0.215 in the transitional and 0.24 in the turbulent regions for all the blade widths; however, it exhibited some sensitivity to variation of blade width in the laminar region.

NOMENCLATURE

C impeller off-bottom clearance (m)
D impeller diameter (m)
n number of blades
N rotational speed (s^{-1})
Np Power number = $P/(N^3D^5\rho)$
Nq flow or pumping number = Qp/ND^3
p pressure (Pa)
P impeller power input (w)
Qp pumping flow rate (m^3s^{-1})
r radial coordinate (m)
Re Reynolds number = $(\rho ND^2)/\mu$
RRF rotating reference frame model
MRF multiple reference frame model
S represents source terms
T tank diameter (m)
T torque (Nm)
u velocity (m/s)
Wb blade width (m)
ρ liquid density (kg/m^3)
μ dynamic viscosity (kg/ms)
η_e pumping effectiveness = Nq/Np
λ_p pumping efficiency= $Nq/(Np)^{1/3}$
$\boldsymbol{\tau}$ stress tensor
$\boldsymbol{\Omega}$ angular velocity of the frame (rad s^{-1})

INTRODUCTION

Mixing operations are of fundamental importance in process industry, where they find many areas of application. The range of applications is diverse and includes the following: blending of two liquids, solid suspension accompanied by another process such as leaching and flotation, gas dispersion into a liquid followed by absorption and/or chemical reaction between liquid and gas, fermentation or crystallisation. Mixing can be defined as an operation that tends to reduce the non-uniformities or gradients in composition, properties, or temperature of material in the bulk. The efficiency of many processes depends on the quality of mixing.

The above tasks are often accomplished by moving material, solid, liquid or gas, within the vessel using an agitator. Uhl and Gray [1] suggested that for fluids the movement occurs by laminar or turbulent mixing culminating in molecular diffusion. In this paper the laminar flow regime was considered to extend beyond the region determined according to the classical definition, i.e. where the Re × Np = -1 (Re is the Reynolds number, plotted on a log scale and Np is the power number). Kuncewicz [2] identified this laminar region as where Re < 70. The fully turbulent region was considered to be where Re ≥ 10^4 and the flow associated with the region between the above two was considered to be in the transitional regime.

A basic mixing system (Figure 1) comprises a vessel or container, which can be baffled or unbaffled, open or covered with a lid, a fluid and sometimes solid particles, and with an agitator mounted on a shaft. The agitator is perhaps the most critical part of the mixing system since it provides the source of mixing energy and determines the type of flow pattern, pumping and circulation flow rates. In practice, no single impeller is sufficiently versatile to perform all the functions of mechanical agitation; as a result impellers are designed or selected to generate a flow pattern that enhances performance for a specific function [3]. It is therefore not surprising that a large number of studies have focused on the redesign of the impeller geometry to achieve energy efficient systems [4, 5].

Previous studies on impeller design have investigated the effect of impeller and tank relative dimensions [6], number of impeller blades [7] and impeller type [8] on global mixing parameters. Wu et al. [9] presented an interesting study of the effect of impeller geometry on velocity and solids suspension in a baffled tank and also

provided a correlation between flow number (Nq = Qp/(ND^3) and power number (Np = P/(ρN^{3}D^5 in the form of circulation efficiency. However, the study was for pitched blade turbines and disc turbines. Recently, Jayanti and Murthy [10] have conducted a detailed numerical study of power and mixing time for paddle impellers. But, they used the standard k-epsilon model for flows at Re = 480 and 960, which fall within the transitional regime, whereas the standard k-epsilon model is more suitable for fully turbulent flow.

The current study has investigated the pumping effectiveness of an unbaffled mixing system equipped with a 6 bladed paddle impeller operating in the laminar, transitional and fully turbulent regimes. The main thrust of the investigation was to study the effect that the impeller blade width has on the flow number, power number, and hence the pumping effectiveness and efficiency.

NUMERICAL METHOD

Governing equations

The equations solved in the simulations are the standard conservation equations of mass and momentum. As the impeller blades move through the fluid, to accurately describe such motion, the momentum equations for the entire domain are solved in a rotating reference frame (RRF). It means that the frame of reference is attached to the impeller, which appears to be stationary while the tank wall, bottom and top ends appear to be moving with the same speed as that of the frame but in the opposite direction. The absence of baffles means that the RRF, rather than the Multiple Reference Frame (MRF) is the preferred option of treating this flow within the FLUENT environment.

Given that the fluid used is incompressible, the modified conservation equations take the form:

$$\nabla \cdot \mathbf{u} = 0\,, \tag{1}$$

$$\nabla \cdot (\rho \mathbf{u}\mathbf{u}) = -\nabla \mathbf{p} + \nabla \boldsymbol{\tau} + \mathbf{s}\,, \tag{2}$$

where $\mathbf{u}$ is the velocity relative to the frame of reference introduced by working in a non-inertial frame, $\boldsymbol{\tau}$ is the stress tensor and $\mathbf{s}$ represents the source terms, i.e. the Coriolis and centrifugal forces,

$$\mathbf{s} = -2\rho\boldsymbol{\Omega} \times \mathbf{u} - \rho\boldsymbol{\Omega} \times (\boldsymbol{\Omega} \times \mathbf{r})\,, \tag{3}$$

where $\boldsymbol{\Omega}$ is the angular velocity of the frame.

Simulated geometry

The mixing vessel system modelled was a laboratory configuration schematically represented by Figure 1. It consisted of a cylindrical tank of diameter T = 0.486 m, filled with silicone oil (kinematic viscosity = 5x10^{-4} m^2/s and density = 969 kg/m^3). The mixing vessel was equipped with a 6 bladed paddle impeller with a diameter D = 0.162 m (T/3). The impeller was located with an off-bottom clearance C = T/3, which has previously been found to be an optimum impeller position; Kuncewicz [2] found that at C = T/3 the total secondary circulation reached the highest value, which would imply that mixing time would be the lowest. In addition, Mishra and Joshi [3] reported that C = T/3 and D = T/3 were associated with the maximum flow number for a disk turbine. The liquid height, H, was equal to the tank diameter T. The blade thickness was 0.008 m. Four impellers with different blade widths (Wb) were employed in simulations and will be referred to as h1, h2, h3 and h4. The different blade widths were normalised with respect to Wb2 (Wb2 = 0.0324 m or 0.2D) as Wb1 = 0.5, Wb3 = 1.5 and Wb4 = 2.0. In terms of tank diameter Wb1 = 0.033T, Wb2 = 0.067T, Wb3 = 0.10T and Wb4 = 0.133T.

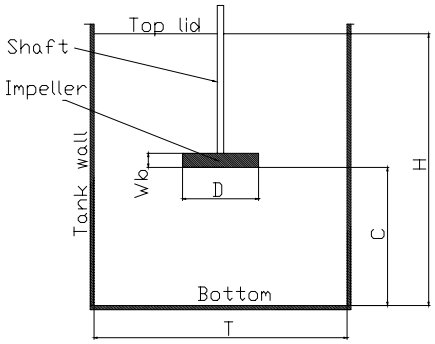

Figure 1. Mixing vessel configuration

Computational grids

A grid resolution study was performed using seven different grid sizes (Table 1) generated with the help of the commercial software GAMBIT (version 2.0). The task of generating so many models was made easier by the use of GAMBIT journal files, which automated the design of geometries and meshing. Since the mixing vessel was agitated by a 6 bladed impeller, only a 60° sector was modelled to take advantage of the rotational symmetry of the geometry. Table 1 shows the characteristics of the seven grids employed in this study. It can be seen that the grid density was varied from 112,358 structured hexahedral cells to 553,348 cells. The grids were compressed near the solid surfaces, especially rotating surfaces of the blade to ensure adequate resolution. For turbulent flow simulations, the grids were adapted in order to further resolve the flow near the wall regions.

	Number of cells (60° sector)			
Grid #	Axial	Radial	Azimuthal	Total
G1	96	52	24	112,358
G2	104	58	26	148,984
G3	116	65	30	211,468
G4	131	70	32	283,904
G5	142	72	30	303,166
G6	133	81	30	310,958
G7	166	95	36	553,348

Table 1: Grid point parameters for the computational grids

Boundary conditions

For the rotating reference frame (RRF) employed in the calculations, the impeller and shaft were set to have zero velocity; the top, bottom and side walls were assigned a rotational velocity equal in magnitude but opposite in sign to the rotation of the frame of reference. All solid surfaces were given a no-slip velocity condition. As previously mentioned, due to the rotational symmetry of the geometry only $1/6^{th}$ of the vessel was modelled. Therefore, a periodic boundary condition was imposed at the two end surfaces in the azimuthal direction.

Turbulence modelling

It is generally agreed in mixing applications that flows characterised by $Re \geq 10^4$ can be regarded as fully turbulent. In this study the turbulent flow regime was investigated at three Reynolds numbers, 10^4, 2×10^4 and 5×10^4. The main turbulence model used here was the two equation standard k-ε model (Launder & Spalding [11]). The enhanced-wall treatment was used at the solid surfaces. The reason for using the enhanced-wall treatment, as opposed to the standard wall functions, was two fold: first, the wall functions are not well suited for flow with strong body forces such as flow near a rotating disk or impeller and second, the enhanced wall treatment can automatically accommodate cells placed in the log-law layer and hence provides a more robust treatment.

In addition to the k-ε model, for $Re = 10^4$, turbulence was also modelled using the Renormalization Group (RNG) k-ε model. The RNG model is another of the two-equation models based on the Reynolds-Averaged Navier-Stokes (RANS) equations. It has been found that the RNG performs better than the standard k-ε model for more complex flows with high strain and swirl as is the case in mixing vessels. The final turbulence model employed in this study was the Reynolds Stress Model (RSM). The RSM model was found to be considerably more costly and difficult to converge than the two-equation models, although it is supposed to be the most accurate model for 3D flows with strong swirl and rotation.

The flows in the transitional region were modelled using the two-equation k-ω turbulence model. This newly incorporated turbulence model, applicable to transitional flows, was based on the shear stress transport (SST) k-ω model developed by Menter [12].

Solution method

As mentioned above, the RRF technique was used for modelling, which meant that a single frame of reference attached to the impeller was considered in solving the equations of motion. The segregated solution algorithm with implicit solver formulation was employed as well as a relative velocity formulation.

As a result of using the segregated solver, the pressure equation was discretized with the help of the PRESTO scheme, which is well suited to highly swirling flows. The other discretization schemes employed were as follows: SIMPLEC for the pressure-velocity coupling and the second-order upwind scheme for the momentum, turbulence kinetic energy and dissipation rate. The under-relaxation factors were generally kept at their default values and were adjusted only when it was necessary to stabilise the solution by controlling convergence.

Convergence monitoring

Convergence was monitored by checking the information from computed residuals of all equations and also by keeping track of surface monitors. Scaled residuals were primarily used. Computations were continued until the values of residuals were progressively reducing by typically five or six orders of magnitude, although in a few cases this could not be achieved. The main convergence monitoring tools employed here were surface monitors. Three surface monitors were used, one for the mass flow rate through a circumferential curved surface at the impeller blade tip radius and two for the integral of static pressure on the leading and trailing sides of the impeller blade. Convergence was considered to have been achieved when values of the three monitors were constant to within ± 0.01% over 500 iterations. Such convergence criteria are very stringent and likely to ensure that the results were fully converged.

Grid adaption

The grids shown in Table 1 were sufficiently dense for laminar flow conditions; however, for turbulent flow conditions grid refinements were required. To better resolve the flow in the near wall regions, especially the rotating walls of the impeller blades, solution adaptive refinements were applied. By adapting the mesh this way cells were added where they were required without affecting the other regions of the flow domain, hence keeping the grid size to an optimum level. Moreover, it is always very difficult to correctly predict the required resolution of the mesh near walls while generating the grid; hence the automatic y^+ adaption is generally the best way to refine the mesh during the solution process. Great care was taken to ensure that the centroid of the first cell near the wall was such that $y^+ \approx 1$, which is the optimum value when using the enhanced wall treatment.

Derived quantities

Using the simulated results the following global mixing parameters were evaluated: the Pumping or Flow Number, Nq, and the Power Number, Np, from which the Pumping Effectiveness (Equation 4) and Pumping Efficiency (Equation 5) were computed:

$$\eta_e = \frac{Nq}{Np} \tag{4}$$

$$\lambda_p = \frac{Nq}{Np^{1/3}} \tag{5}$$

Np, as defined above, is the dimensionless form of the power required to rotate the impeller ($P=2\pi NnT$). The torque (T) exerted on one blade was evaluated in the Fluent environment as a "custom field function" using CFD pressure data on both sides according to Equation (6):

$$T = \sum_i (\Delta p)_i A_i r_i \tag{6}$$

where n is the number of blades, A_i is the projected surface area of the elemental surface "i" on the blade leading or trailing face, r_i is the corresponding radial location and Δp_i is the elemental pressure difference between the leading and trailing faces of the blade (Nm^{-2}).

RESULTS

Flow field results showing predicted velocity fields on radial planes are presented in this section. Other results depict the relationship between the pumping and power numbers, the pumping effectiveness and efficiency, on one hand, and the Reynolds number and normalised impeller blade width, on the other hand. Some of the predicted results were compared with Nagata's classical results for an 8 bladed paddle impeller with diameter D = T/2 and a blade width equal to 0.10T, which roughly corresponds here to the impeller h3 (Wb3 = 0.10T but with 6 blades and D = T/3). It is further planned to compare the numerical predictions presented here with results from experiments currently in progress.

A grid resolution study was conducted using the grids shown in Table 1 by monitoring the mass flow rate through a circumferential surface located at the impeller tip radius and also the pressure difference between the leading and trailing faces of the blade. It was found that grid G6 (310,958 cells) was the most optimal and was therefore used in the computations.

Flow Field

Figures 2 (a) and (b) show the predicted velocity vector fields for laminar flow (Re = 10) and transitional flow (Re = 100) conditions respectively. The flow fields are shown on a radial plane passing through the mid-plane of the impeller blade in the middle of the computation domain.

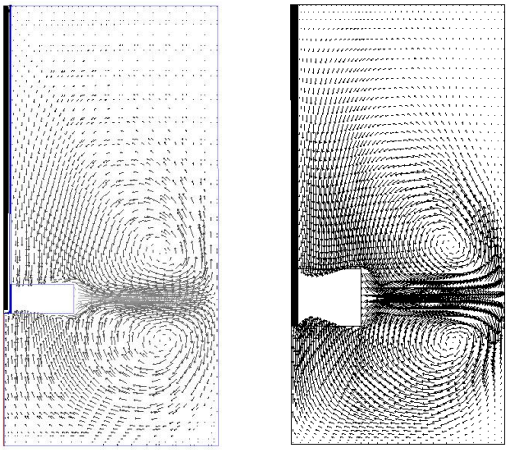

(a) (b)

Figure 2: Radial and axial velocity vector plots of the predicted flow fields: (a) for impeller h1 at Re=10; (b) for impeller h4 at Re=100

Examination of the flow patterns reveals, for both cases, a radial jet emanating from the impeller and directed towards the tank vertical wall. Upon approaching the wall this radial jet is deflected, producing two streams, one moving vertically upwards and the other in the opposite direction towards the tank bottom surface. The presence of the two solid surfaces, at the bottom and top, causes the jets to turn towards the axis of rotation before returning to the impeller region. The above fluid motion is responsible for the two circulation loops. The absence of a free surface prevented the formation of a vortex. The flow is predominantly circumferential, with the region near the impeller shaft having the mean tangential velocity directly proportional to the radius and decreasing towards the tank wall in the outer region.

It can be seen from the two velocity fields (Figures 2 (a) and (b)) that for laminar flow a small and weak recirculation loop is formed with nearly dead regions away from the impeller. As the impeller speed increases, the transitional flow pattern shows an increase in strength and size of the recirculation loop, hence a reduction in the dead zone area. For much higher Reynolds numbers, the flow patterns revealed strong recirculation covering the entire tank region. The above differences in flow patterns support findings by other workers [13, 14] that the product of the mixing time and the impeller rotational speed is higher for laminar flow than for turbulent flow.

Pumping Capacity

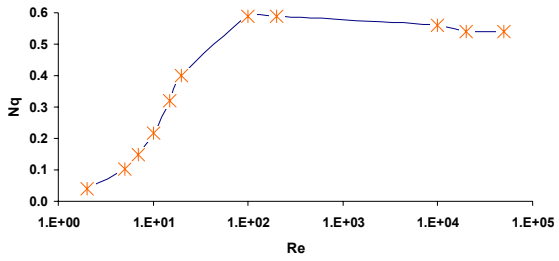

Figure 3: Variation of the flow number with Reynolds number for the impeller h2

Figure 3 shows the characteristic flow curve for the impeller h2. It can be seen that the flow number (Nq) is very low for laminar flow and increases with increasing Re. A salient feature in this graph is that the Nq reaches a maximum value in the transition region, specifically at Re ≈ 200. In the turbulent flow regime Nq appears to be constant at 0.55. This trend is in agreement with the characteristic flow curve published by Nagata [13] for an 8 bladed paddle impeller.

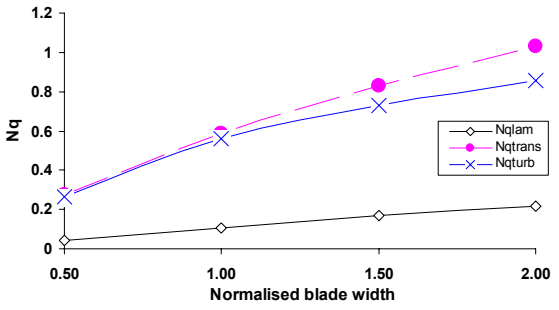

Figure 4: Flow number as a function of impeller blade width for: laminar (Re=5); transitional (Re=100) and turbulent ($Re=10^4$) flow regimes

Nagata's Nq was 0.34, for a fully turbulent flow, whereas the flow number for the impeller h3 operating in fully turbulent regime was found to be 0.729 (Figure 4). The disparity is due to differences in the impeller diameter and number of blades used in the two studies. Figure 4 shows the effect of varying the blade width on Nq considering a representative Re for each flow regime. It is obvious that for all blade widths considered, in the laminar flow regime the Nq values were much lower compared with Nq values for either the transition or the turbulent flow regimes. Figure 4 also reveals that the Nq is highest in the transition region as observed from Figure 3.

Power Consumption

The predicted results of Np against Re for the impeller h2 are shown in Figure 5. In the laminar region, the Np decreases as the Re increases, almost linearly especially for Re ≤ 7, in accordance with what most researchers have reported in the past [2, 13]. The Np keeps decreasing in the transition region until it reaches a constant value of about 2.3 in the turbulent flow region (Re ≥ 10^4). The value of Np for the impeller h3 was predicted to be approximately 3.04 (Figure 6), which is in close agreement with the value of 3.4 computed by Jayanti and Murthy [10] using Nagata's [13] correlation.

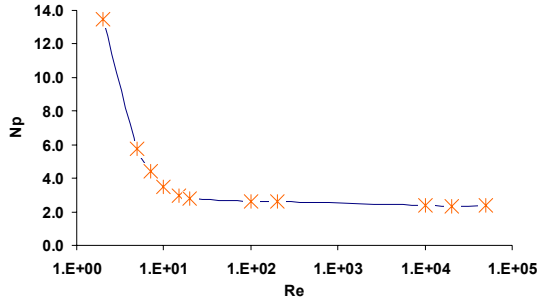

Figure 5: Variation of the power number with Reynolds number for the impeller h2

In Figure 6, the variation of Np with the blade width (Wb) is reported for laminar, transitional and turbulent flow regimes. It is evident that an increase in impeller blade width results in an increase in Np, however in the turbulent region this effect is relatively less significant. For all the blade widths considered here Np is highest in the laminar region and the lowest in the turbulent regime, which agrees with Figure 5.

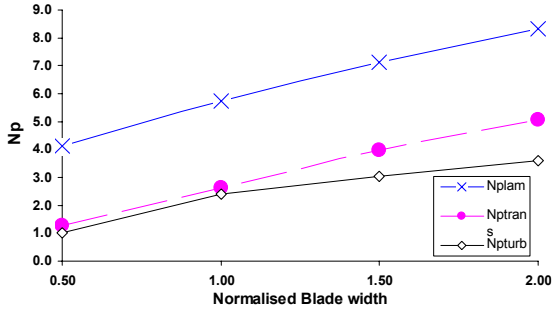

Figure 6: Power number as a function of impeller blade width for: laminar (Re=5); transitional (Re=100) and turbulent (Re=10^4) flow regimes

Pumping Effectiveness and Efficiency

A useful index often used to characterize the effectiveness of an agitator in a mixing process is the pumping effectiveness, η_e (Equation 4). Another useful correlation is the circulation or pumping efficiency, λ_p, (Equation 5), previously used by Wu et al. [9] for disc turbines.

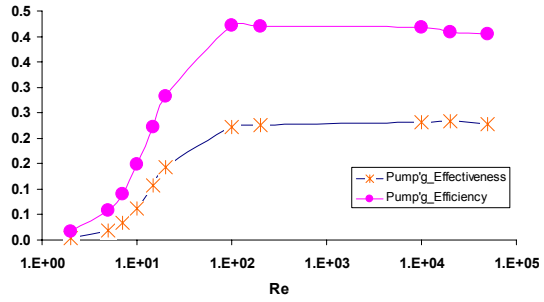

Figure 7: Comparison between pumping effectiveness and pumping efficiency at different flow regimes (impeller h2)

Figure 7 shows the variation of both the pumping effectiveness and pumping efficiency with respect to Re for the impeller h2. Both parameters tend to vary in a similar way, from low values in the laminar region increasing until maximum values (η_e=0.23 & λ_p=0.41) in the transition region. In the turbulent region the two parameters maintain almost their maximum values. The value of λ_p=0.41 found here compares very well with the value of 0.42 reported by Wu et al. (2001) for radial disc turbines.

Figure 8 shows the pumping effectiveness as a function of the impeller blade width. The salient feature of Figure 8 is that except for the laminar case, η_e is almost constant at approximately 0.215 in the transitional and 0.24 in the turbulent flow regimes irrespective of the blade width. In the laminar regime, an increase in blade width generates a corresponding increase in η_e, with the biggest effect noted from h1 to h2, i.e. the ratio of η_e =1.8, whereas from h2 to h2 and h3 to h4 the ratio is about 1.1. Such a progression suggests that an optimum value of Wb would be reached where further increases would result in a decrease in η_e.

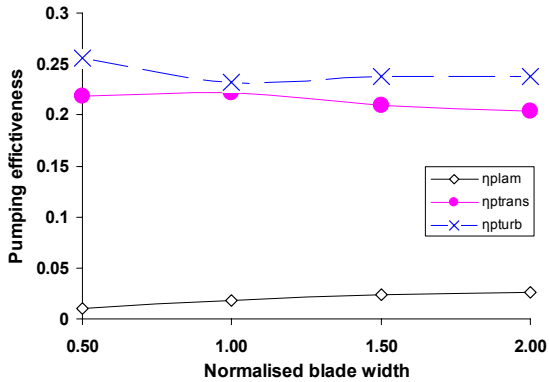

Figure 8: Predicted effect of impeller blade width on the pumping effectiveness for: laminar (Re=5); transitional (Re=100) and turbulent (Re=10^4) flow regimes.

Figure 9 shows that λ_p tends to increase with an increase in blade width in all flow regimes. The ratio between

successive pumping efficiencies decreases as the blade width increases. In the transitional and turbulent flow regimes the λ_p appears to have almost the same values for corresponding blade widths.

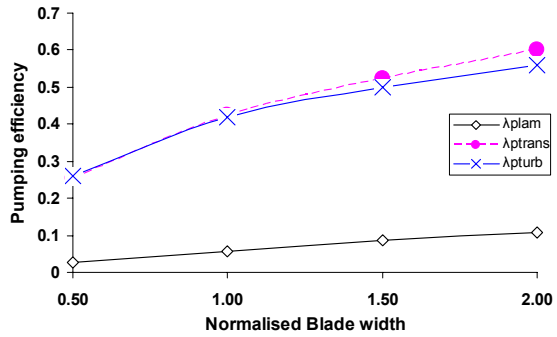

Figure 9: Predicted effect of impeller blade width on the pumping efficiency for: laminar (Re=5); transitional (Re=100) and turbulent (Re=10^4) flow regimes.

Effect of turbulence model

Turbulence model	Nq	Np	η_e	λ_p
Std. k-ε	0.56	2.41	0.23	0.42
RNG k-ε	0.49	1.94	0.25	0.39
RSM	0.46	1.89	0.24	0.37

Table 2: Predicted results using three different turbulence models for the impeller h2 at Re=10^4

Predicted results for Nq, Np, η_e and λ_p obtained using the standard k-ε, RNG k-ε and RSM turbulence models are shown in Table 2. All the results are for a mixing model, fitted with the impeller h2 and operated at Re = 10^4. Compared with the RSM results, the other models predict values which are 5% to 25% higher.

CONCLUSIONS

The paper has presented numerical modelling of flow in an unbaffled vessel agitated by a 6 bladed paddle impeller. The rotating reference frame method was employed in the solution process. Numerical predictions of the variation of Nq, Np, η_e and λ_p with Re and blade width have been presented. Some results have been compared with classical data of Nagata [13] and other researchers' findings and agreements have been found to be generally good. From the results the following conclusions can be drawn:

- The predicted characteristic curves for Nq and Np have shown similar trends to previous results.
- Increases in blade width have been seen to result in corresponding increases in Nq, Np and λ_p, at least for the range of blade widths covered here.
- For all widths considered here Np was highest in the laminar region and lowest in the turbulent region, whereas Nq was highest in the transitional and reduced in value slightly in the turbulent region.
- Pumping efficiency was found to be constant at 0.215 in the transitional and 0.24 in the turbulent regions; however, it exhibited some sensitivity to variation of blade width in the laminar region.
- Further validation and simulations using the RNG k-ε and RSM turbulence models are required.

REFERENCES

1. UHL, V.W. and J.B. GRAY, *Mixing: Theory and practice*. Vol. I. 1966: Academic Press. 340.
2. KUNCEWICZ, C., *Three-dimensional model of laminar liquid flow for paddle impellers and flat-blade turbines.* Chemical Engineering Science, 1992. **47**(15-16): P. 3959-3967.
3. MISHRA, V.P. and J.B. JOSHI, *Flow generated by a disc turbine: part III. Effect of impeller diameter, impeller location and comparison with other radial flow turbines.* Chemical Engineering Research & Design, 1993. **71**(A5): p. 563-573.
4. PAPASTEFANOS, N. and M. STAMATOUDIS, *Effect of vessel and impeller geometry on impeller power number in closed vessels for Reynolds numbers between 40 and 65000.* Chemical Engineering Research & Design, 1989. **67**(2): p. 169-174.
5. ROBERTS, R.M., M.R. GRAY, B. THOMPSON, and S.M. KRESTA, *The Effect of Impeller and Tank Geometry on Circulation Time Distributions in Stirred Tanks.* Chemical Engineering Research & Design, 1995. **73**(A1): p. 78-86.
6. IBRAHIM, S. and A.W. NIENOW, *Power curves and flow patterns for a range of impellers in Newtonian fluids: 40 less than Re less than 5 multiplied by 105.* Chemical Engineering Research & Design, 1995. **73**(A5): p. 485-491.
7. LU, W.M. and B.S. YANG, *Effect of Blade Pitch on the Structure of the Trailing Vortex around Rushton Turbine Impellers.* Canadian Journal of Chemical Engineering, 1998. **76**(3): p. 556-562.
8. BAKKER, A. and H.E.A. VAN DEN AKKER, *Single-phase flow in stirred reactors.* Chemical Engineering Research & Design, 1994. **72**(A4): p. 583-593.
9. WU, J., Y. ZHU, and L. PULLUM, *Impeller geometry effect on velocity and solids suspension.* Chemical Engineering Research & Design, 2001. **79**(A8): p. 989-997.
10. JAYANTI, S. and S. MURTHY, *CFD study of power and mixing time for paddle mixing in unbaffled vessels.* Chemical Engineering Research and Design, 2002. **80**: p. 482-498.
11. LAUNDER, B.E. and D.B. SPALDING, *The numerical computation of turbulent flows.* Computer Methods in Applied Mechanics and Engineering, 1974. **3**(2): p. 269-289.
12. MENTER, F.R., *Two-equation eddy-viscosity turbulence models for engineering applications.* AIAA Journal, 1994. **32**(8): p. 1598-1605.
13. NAGATA, S., *Mixing Principles and Applications*. 1975, New York: John Wiley & Sons. 458p.
14. STEIN, W.A., *Mixing times in bubble columns and agitated vessels.* International Chemical Engineering, 1992. **32**: p. 449-474.